Comptes Rendus
Chimie
Supplementary material to the article available at:
https://doi.org/10.5802/crchim.113

Supplementary material: Zinc phthalocyanine absorbing in the near-infrared with application for transparent and colorless dye-sensitized solar cells

Thibaut Baron [a], Ximena Zarate [*, b], Yoan Hidalgo-Rosa [c], Michael Zambrano-Angulo [d], Kevin Mall-Haidaraly [a], Ricardo Pino-Rios [d], Yann Pellegrin [a], Fabrice Odobel [*, a] and Gloria Cárdenas-Jirón [*, d]

[a] Université de Nantes, CNRS, CEISAM UMR 6230, F-44000 Nantes, France

[b] Instituto de Ciencias Químicas Aplicadas, Facultad de Ingeniería, Universidad Autónoma de Chile, Santiago, Chile

[c] Doctorado en Fisicoquímica Molecular, Universidad Andres Bello, Santiago, Chile

[d] Laboratory of Theoretical Chemistry, Faculty of Chemistry and Biology, University of Santiago de Chile (USACH), Santiago, Chile

E-mails: thibaut.baron@univ-nantes.fr (T. Baron), ximena.zarate@uautonoma.cl (X. Zarate), yoanhrj@gmail.com (Y. Hidalgo-Rosa), michael.zambrano@usach.cl (M. Zambrano-Angulo), kevin.mallhaidaraly@gmail.com (K. Mall-Haidaraly), ricardo.pino@usach.cl (R. Pino-Rios), Yann.Pellegrin@univ-nantes.fr (Y. Pellegrin), Fabrice.Odobel@univ-nantes.fr (F. Odobel), gloria.cardenas@usach.cl (G. Cárdenas-Jirón)

1. General

^{1}H and ^{13}C NMR spectra were recorded on an *AVANCE 300 MHz BRUKER, AVANCE III 400 MHz BRUKER*. Chemical shifts for 1H NMR spectra are calibrated on residual protons in the deuterated solvent (**CDCl$_3$** δ = 7.26 ppm for ^{1}H and δ = 77.16 ppm for ^{13}C). Spectra were recorded at room temperature, chemical shifts are given in ppm and coupling constants in Hz.

High-resolution mass (HRMS) spectra were obtained by electrospray ionization coupled with high resolution ion trap orbitrap (LTQ-Orbitrap, ThermoFisher Scientific,) working in ion-positive or ion-negative mode. Electrochemical measurements were performed with a potentiostat-galvanostat *Autolab PGSTAT 302N* controlled by resident GPES software (General Purpose Electrochemical System 4.9) or NOVA software using a conventional single-compartment three-electrodes cell. The working electrode was a glassy carbon one. The auxiliary electrode was a stainless wire and the reference one was the saturated potassium chloride calomel electrode (SCE). The supporting electrolyte was 0.1 N Bu_4NPF_6 in DMF and solutions were purged with argon before the measurements. All potentials are quoted relative to SCE. In all the presented experiments the scan rate was 100 mV/s.

UV-Visible absorption spectra were recorded on a *UV-2401PC Shimadzu* spectrophotometer using 1 cm path length cells. Emission spectra were recorded

* Corresponding authors.

on a SPEX Fluoromax-4 Jobin Yvon fluorimeter (1 cm quartz cells). Emission spectra are corrected in near-infrared part.

2. Photovoltaic cell fabrication

Conductive glass substrates (F-doped SnO_2) were purchased from Pilkington (TEC8, sheet resistance 8 Ω/square). Conductive glass substrates were successively cleaned by sonication in soapy water, then ethanol for 10 min before being fired at 450 °C for 30 min. Once cooled down to room temperature, FTO plates were rinsed with ethanol and dried in ambient air. A first treatment was applied by immersion for 30 min in an aqueous $TiCl_4$ solution (0.3 mL of pure $TiCl_4$ in 500 mL of deionized water) at 80 °C. Layers of TiO_2 were then screen printed with transparent colloidal paste 18NR-T (from Dyesol), with drying steps at 150 °C for 20 min between each layer. A final light scattering overlayer was eventually screen printed (18NR AO, Dyesol) over the transparent layer. The obtained substrates were then sintered at 450 °C, following a progressive heating ramp (135 °C for 15 min, 325 °C for 5 min, 375 °C for 5 min, 450 °C for 30 min). A second $TiCl_4$ treatment was applied while cells are still hot, followed by a final firing at 450 °C for 30 min. The prepared TiO_2 electrodes were soaked while still hot (80 °C) in a solution of **KMH63** (0.2 mM in a mixture Toluene/MeOH, 1/1) with or without CDCA (see manuscript text) for one night and finally rinsed with the mixture Toluene/MeOH: 1/1.

Pt counter-electrodes were prepared by chemical deposition of platinum from hexachloroplatinic acid in distilled isopropanol (10 mg/mL) and sintered at 380 °C in the oven for 30 minutes. The photoelectrode and the counter-electrode were placed on top of each other using a thin transparent film of Surlyn® polymer (DuPont, 60 µm), as a spacer to form the electrolyte space. The empty cell was tightly held, and the edges were heated to 110 °C to seal the two electrodes together. A drop of electrolyte was introduced through a predrilled hole in the counter electrode by vacuum backfilling, and was sealed afterward. The cell had an active area of *ca.* 0.25 cm^2.

The two electrodes were placed on top of each other using a thin transparent film of Surlyn polymer (DuPont, 60 µm) as a spacer to form the electrolyte space. The empty cell was tightly held, and the edges were heated to 110 °C to seal the two electrodes together. A drop of electrolyte was introduced through a predrilled hole in the counter electrode by vacuum backfilling, and was sealed afterward. The cell had an active area of *ca.* 0.25 cm^2.

The current-voltage characteristics were determined by applying an external potential bias to the cell and measuring the photocurrent using a Keithley model 2400 digital source meter. The solar simulator is an Oriel Lamp calibrated to 100 mW/cm^2. The photovoltaic measurements were recorded on unmasked cells. The overall conversion efficiency (PCE) of the photovoltaic cell is calculated by multiplying the short circuit photocurrent density (J_{sc}), the open-circuit photovoltage (V_{oc}), the fill factor of the cell (FF), and dividing by the intensity of the incident light (AM1.5, 100 mW cm^{-2}).

3. Preparation of 5

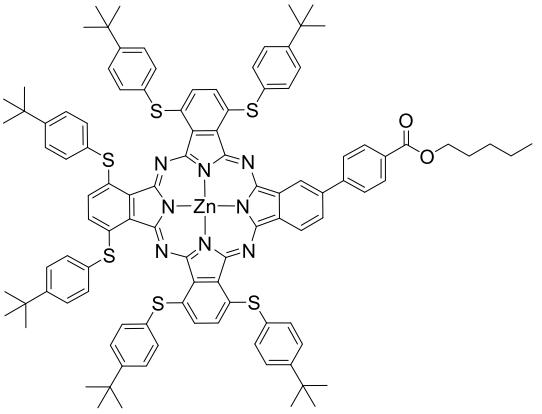

In a sealed tube, 200 mg (0,44 mmol, 3 eq) of **3**, 45 mg (0,15 mmol, 1 eq) of **4** and 67 mg (0,37 mmol, 2.5 eq) of $Zn(OAc)_2$ were put under argon. 3 mL pentanol was added in the tube and the mixture was heated at 100 °C until dissolution. 0,25 mL DBU was added dropwise and the reaction mixture was refluxed at 140 °C overnight. The reaction was then brought back to room temperature, quenched with H_2O, extracted with CH_2Cl_2, washed with H_2O and the solvent was evaporated under vacuum. The crude was filtrated under MeOH. A green powder was afforded by purification on an automated column (silica gel, Toluene/THF/Pyridine (9,3:0,35:0,35) (v:v:v)) plus a purification by recycling HPLC and finally a purification by preparative TLC (silica, Toluene/THF/Pyridine (9,3:0,35:0,35) (v:v:v)) (0.023 g, 9%).

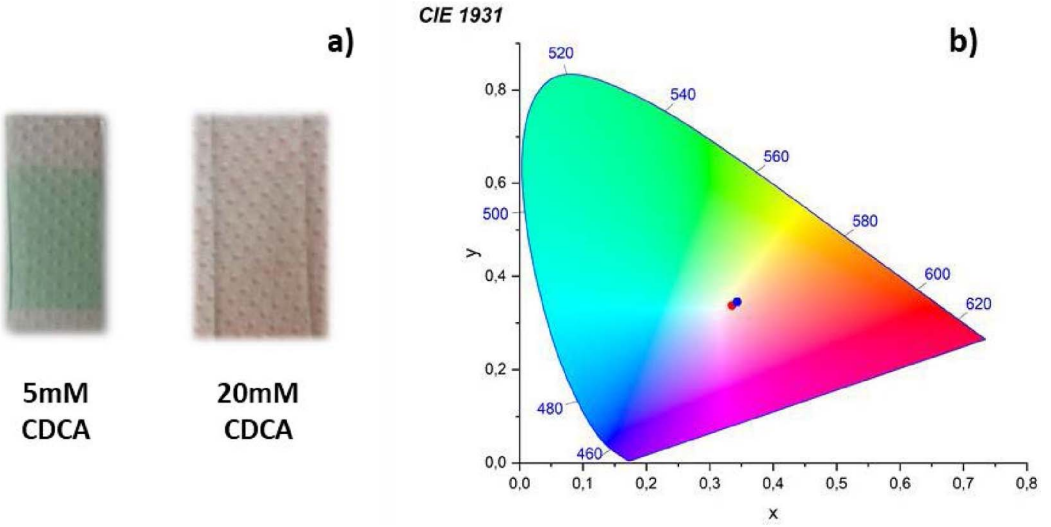

Supplementary Figure S1. (a) Pictures of thin mesoporous TiO_2 film without scattering layer coated with **KMH63** along with 5 mM (left) and 20 mM (right) of CDCA in the dye bath. (b) Representation of the CIE 1931 color space diagram of these two electrodes with 5 mM (0.33507, 0.33792) and 20 mM (0.34314, 0.3455) of CDCA.

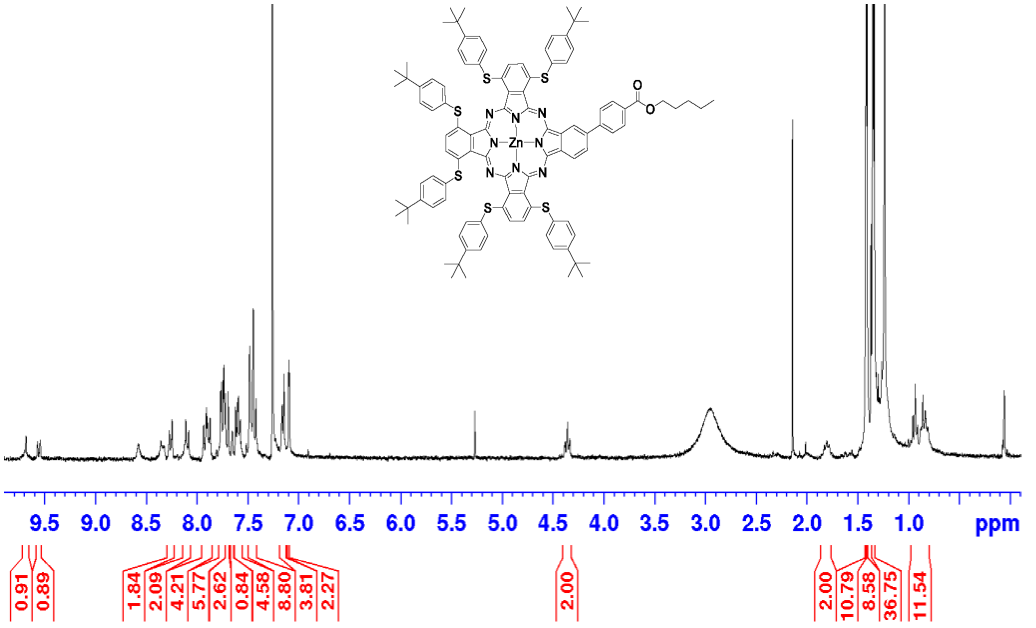

Supplementary Figure S2. ^{1}H NMR (300 MHz, $CDCl_3$) spectrum of 5.

MW ($\mathbf{g \cdot mol^{-1}}$): 1753.75

NMR (^{1}**H**, **CDCl**$_3$,

300 MHz) $\boldsymbol{\delta}$ (**ppm**): 9.67 (d, ^4J = 0.78 Hz, 1H), 9.56 (d, ^3J = 7.79 Hz, 1H), 8.26 (d, ^3J = 8.39 Hz, 2H), 8.09 (d, ^3J = 8.43 Hz, 2H), 7.92 (d, ^3J = 8.41 Hz, 2H), 7.90 (d, ^3J = 8.38 Hz, 2H), 7.74 (dd, ^3J = 8.28 Hz, ^4J = 2.32 Hz, 6H), 7.70 (d, ^3J = 8.43 Hz, 2H), 7.65 (s, 1H), 7.59 (m, 4H), 7.45 (m, 8H), 7.15 (m, 4H), 7.09 (d, ^4J = 1.49 Hz, 2H), 4.36 (t, ^3J = 6.46 Hz, 2H), 1.80 (m,

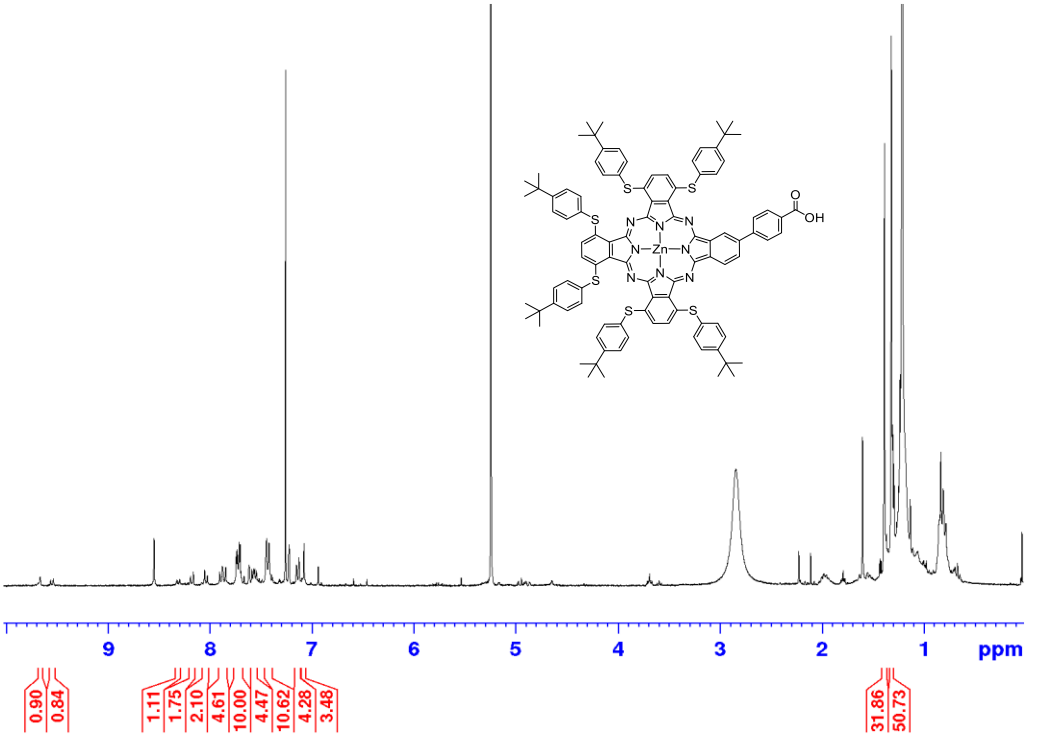

Supplementary Figure S3. ^{1}H NMR (300 MHz, $CDCl_3$) spectrum of **KMH63**.

2H), 1.42 (s, 9H), 1.40 (s, 9H), 1.34 (m, 36H), 0.89 (m, 12H).

HRMS (**ES**+) **m**/**z**: $[M + 2H]^{2+}$ calculated for $C_{104}H_{104}N_8O_2S_6{}^{64}Zn$: 1752.5898; found: 1752.5834. $\Delta = -3.7$ ppm.

4. Preparation of KMH63

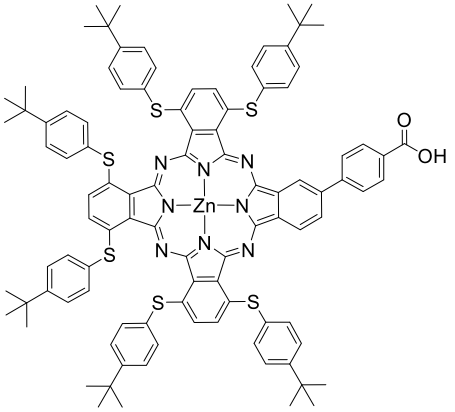

19,2 mg (0.011 mmol) of **5** was dissolved in 5 mL THF. 1 mL (0,11 mmol, 10 eq) of a solution of KOH in 2 mL H_2O was added, the mixture was refluxed at 90 °C. After 24 h, the mixture was brought back to room temperature, neutralized with HCl (2M), extracted with CH_2Cl_2 and the solvent was evaporated under vacuum. A green powder was afforded by precipitation and filtration in petroleum ether (0.018 g, 56%).

MW (**gc**·**mol**$^{-1}$): 1683.62

NMR(^{1}**H**, **CDCl**$_3$, **300 MHz**) $\boldsymbol{\delta}$(**ppm**): 9.67 (s, 1H), 9.55 (d, ^{3}J = 8.45 Hz, 1H), 8.32 (dd, ^{3}J = 8.00 Hz, ^{4}J = 1.60 Hz, 1H), 8.18 (d, ^{3}J = 8.31 Hz, 2H), 8.04 (d, ^{3}J = 8.33 Hz, 2H), 7.87 (m, 4H), 7.72 (dd, ^{3}J = 8.34 Hz, ^{4}J = 2.57 Hz, 10H), 7.57 (m, 4H), 7.43 (dd, ^{3}J = 8.43 Hz, ^{4}J = 2.62 Hz, 10H), 7.14 (m, 4H), 7.08 (m, 3H), 1.38 (s, 18H), 1.32 (s, 36H).

HRMS (**ES**+) **m**/**z**: $[M + 2H]^{2+}$ calculated for $C_{99}H_{94}N_8O_2S_6{}^{64}Zn$: 1682.5115; found: 1682.5070. $\Delta = -2.7$ ppm.

5. Electrochemical part

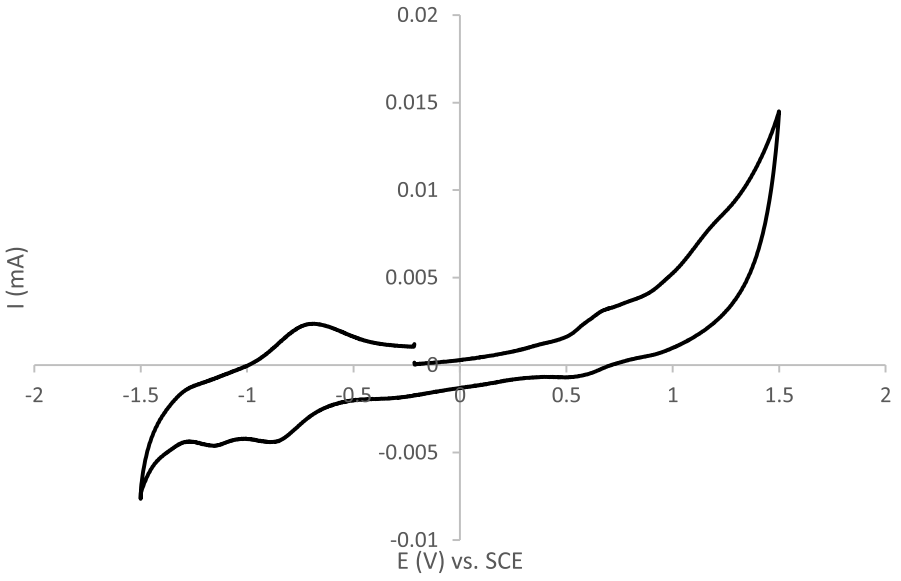

Supplementary Figure S4. Electrochemical properties of **KMH63** in supporting electrolyte (0.1 N Bu_4NPF_6 in DMF), scan rate = 100 mV/s.

6. Emission properties

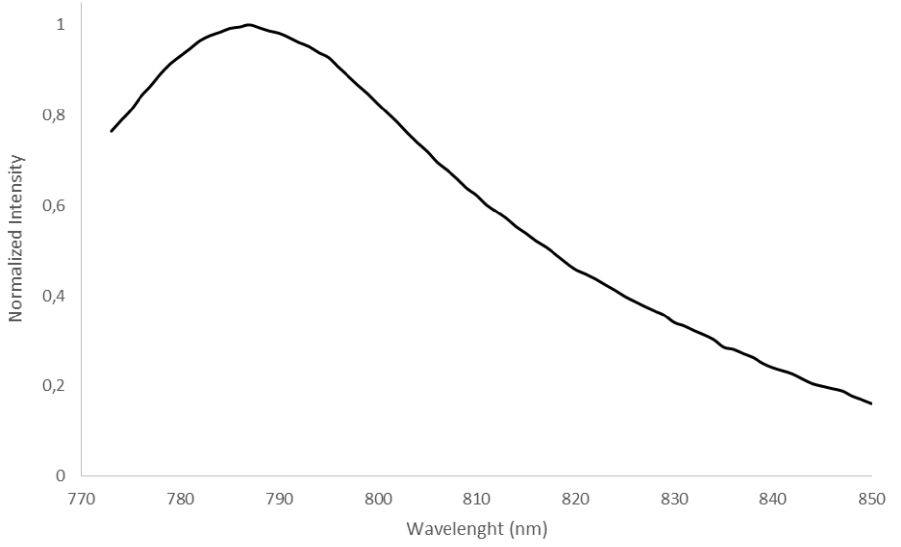

Supplementary Figure S5. Fluorescence spectra of **KMH63** recorded in dichloromethane solution, λ_{excit} = 772 nm.

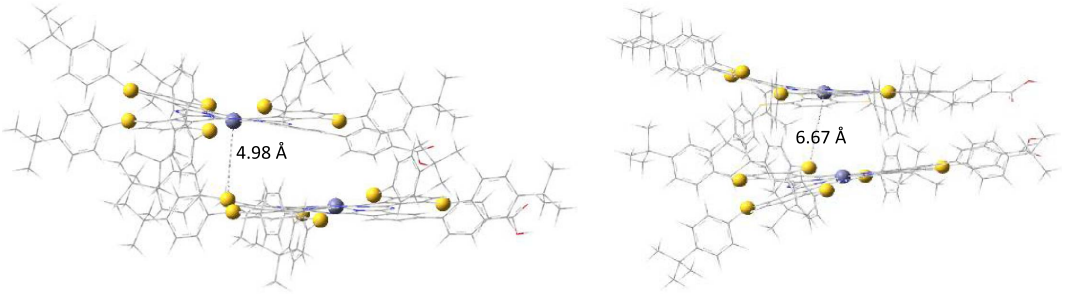

Supplementary Figure S6. Calculated structures of zinc phthalocyanine dimer J (left) and zinc phthalocyanine dimer H (right).

7. Computational study

Full molecular geometry optimization was performed for the ground state of **KMH63** using density functional theory (DFT) with the functional B3LYP [1–3] and the Pople 6-31G(d,p) basis set. The minimum energy structure obtained from the calculations was verified through the calculation of the vibrational frequencies, obtaining a positive value for each of them. The B3LYP functional was used to obtain the geometry of minimum energy because in previous works, it was used for porphyrins and analogous systems [4–6] obtaining a good agreement between the theoretical properties and the experimental data.

In order to assess the influence of the substituents, an aromaticity analysis of the "*internal cross*", six- and five-membered rings of **KMH63** and **ZnPc-BZA** has been carried out. Recently the need for the use of multiple criteria for a complete understanding of aromaticity has been highlighted [7]. Since both systems present aromatic behaviour, the module of magnetically induced current density (MICD) has been initially analyzed. The results can be seen in Figure S6, where it is possible to distinguish in **ZnPc-BZA** (left) the diatropic currents corresponding to the *internal cross* of the macrocycle and the 6MR, according to their aromatic character.

On the other hand, the MICD module shows that for **KMH63** (Figure S6, right), the ring currents of the 6MR cannot be distinguished because they are out of molecular plane, due to the influence of the substituent groups. Additionally, the current in the *internal cross* loses homogeneity and becomes slightly weaker in certain zones, showing that the substituent groups also influence the aromaticity of the macrocycle. To quantify this influence, values of NICS and $NICS_{zz}$ have been obtained, being the differences more noticeable in the latter. The indices were measured in the geometric centers of the different rings in the macrocycle. For the case of the *internal cross*, less negative values (weaker) are observed for the case of **KMH63** with respect to **ZnPc-BZA**, indicating a reduction in aromaticity, as a result of the influence of the substituents added. In the case of the 5MR these are non-aromatic, however, they present positive values which are due to the coupling of the diatropic currents of the aromatic rings that surround it.

The 5MR-2 in **KMH63** presents a very noticeable difference with respect to the others, due to the position of the substituents, the symmetry of the macrocycle and the variations of the diatropic currents surrounding it. With respect to the 6MRs, a reduction in aromaticity can also be seen in the 6MR 1-3 (See Figure S6), which present substituent groups. The 6MR-4 present similar values for **KMH63** and **ZnPc-BZA** denoting a similar aromatic character because they have not been influenced by the S-t-but-phenyl substituent and are more aromatic than the other 6MR.

To confirm the results obtained with the magnetic criteria, the delocalization and geometric criteria. Table S1 shows first the values of the AV1245 index, which indicate that the *internal cross* of **KMH63** is notably less aromatic than **ZnPc-BZA**, with differences of 0.244 a.u. in agreement with NICS and $NICS_{zz}$ calculations. This difference can also be noted for the 6MR, where the values of AV1245, MCI and PDI are higher for **ZnPc-BZA** than **KMH63**, suggesting higher aromaticity, especially in the 6MR-4 because they are not influenced by the substituent. This is also observed through the geometric criterion due to the lower HOMA values of **ZnPc-BZA** with respect to **KMH63**.

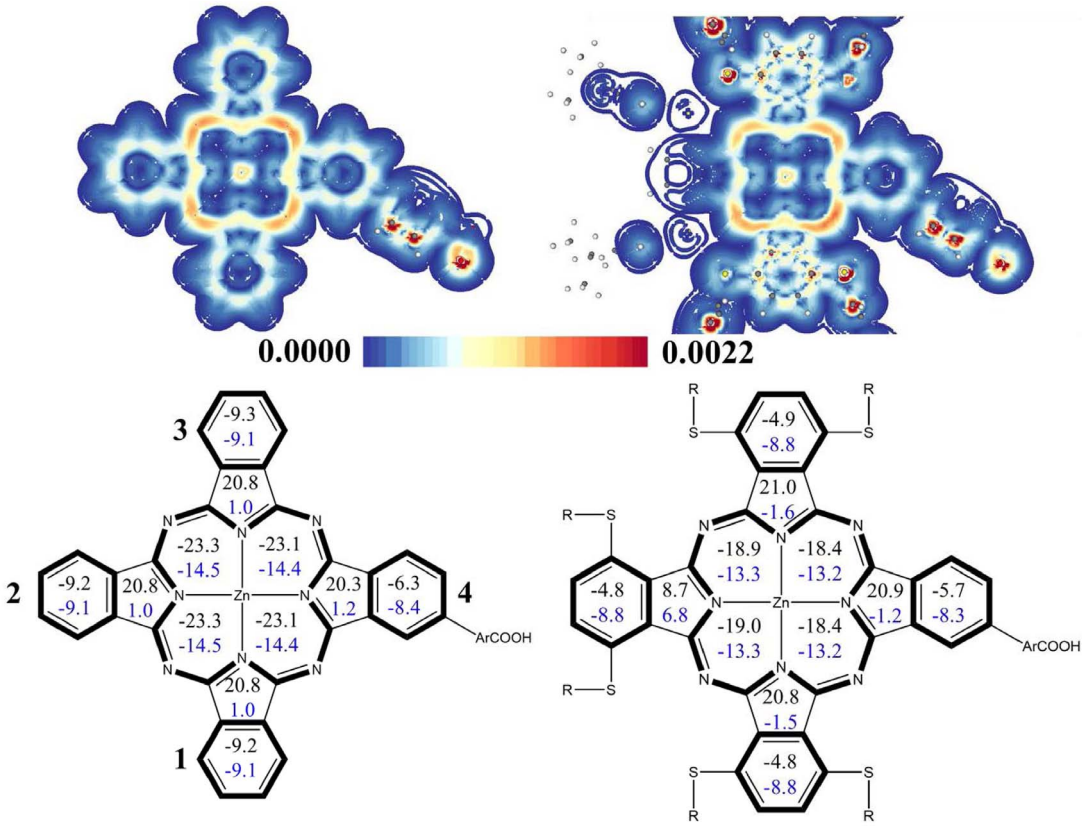

Supplementary Figure S7. (Top) Plots of the module (in a.u.) of the magnetically induced current density at 1.0 a.u. above the molecular plane. (Bottom) $NICS_{ZZ}$ (black) and NICS (blue) values (in ppm) at different geometric centers for phtalocyanines studied in this work at the GIAO-B3LYP/6-31G(d,p) level. R = t-butphenyl. Aromatic internal cross and 6MR have been denoted in bold.

Supplementary Table S1. Values for indexes based on delocalization and geometric criteria at the B3LYP/6-31G(d,p) level

Compound	Ring	AV1245	MCI	PDI	HOMA
ZnPc-BZA	*Internal cross*	1.767	—	—	0.928
	6MR-1	11.812	0.064	0.085	0.955
	6MR-2	11.832	0.064	0.085	0.956
	6MR-3	11.821	0.064	0.085	0.955
	6MR-4	10.692	0.058	0.078	0.928
KMH63	*Internal cross*	1.523	—	—	0.933
	6MR-1	9.647	0.051	0.071	0.915
	6MR-2	9.612	0.051	0.071	0.910
	6MR-3	9.653	0.052	0.071	0.914
	6MR-4	10.628	0.058	0.078	0.927

References

[1] A. D. Becke, *Phys. Rev. A*, 1988, **38**, 3098-3100.
[2] C. Lee, W. Yang, R. G. Parr, *Phys. Rev. B*, 1988, **37**, 785-789.
[3] A. D. Becke, *J. Chem. Phys.*, 1993, **98**, 5648-5652.
[4] G. I. Cárdenas-Jirón, P. Leon-Plata, D. Cortes-Arriagada, J. M. Seminario, *J. Phys. Chem. C*, 2011, **115**, 16052-16062.
[5] M. I. Menéndez, R. López, M. Yañez, G. Cárdenas-Jirón, *Theoret. Chem. Acc.*, 2016, **135**, article no. 122.
[6] R. Urzúa-Leiva, R. Pino-Rios, G. Cárdenas-Jirón, *Phys. Chem. Chem. Phys.*, 2019, **21**, 4339-4348.
[7] R. Báez-Grez, R. Pino-Rios, *New J. Chem.*, 2020, **44**, 18069-18073.